The 8th European Congress on Computational Methods in Applied Sciences and Engineering
ECCOMAS Congress 2022
5 – 9 June 2022, Oslo, Norway

A MODIFIED COHESIVE ZONE MODEL FOR THE SIMULATION OF MIXED-MODE FRACTURE OF CO-CONSOLIDATED THERMOPLASTIC LAMINATES CONSIDERING FIBER BRIDGING

IOANNIS SIOUTIS[*] AND KONSTANTINOS TSERPES[*]

[*]Laboratory of Technology & Strength of Materials,
Department of Mechanical Engineering & Aeronautics,
University of Patras, Patras 26504, Greece
e-mail: kitserpes@upatras.gr

Key words: Thermoplastics, Co-consolidated joints, Fracture toughness, Cohesive Zone Modelling, Finite Element Analysis

Abstract. Fiber bridging is a mechanism that may significantly alter the fracture behavior of composite laminates, adhesively bonded laminates, welded laminates, and co-consolidated laminates. It is therefore quite important for the finite element to take that mechanism into consideration. Such models have been developed for thermosetting laminates; however, this is not the case for thermoplastic laminates and thermoplastic joints. In the present work, a numerical model based on the cohesive zone modelling (CZM) approach has been developed to simulate mixed-mode fracture of co-consolidated thermoplastic laminates by considering fiber bridging. A modified traction separation law of tri-linear form has been developed by superimposing the bi-linear behaviors of the matrix and fibers. Initially, the data from mode I (DCB) and mode II (ENF) fracture toughness tests were used to construct the R-curves of the joints in the opening and sliding directions. The aforementioned curves were embedded into the numerical models through a user-defined material subroutine developed in the LS-Dyna FE code, in order to extract the fiber bridging law directly from the simulation results. The model was used to simulate fracture of a Single-Lap-Shear (SLS) specimen in which a considerable amount of fiber bridging was observed on the fracture area. The numerical results show that the developed model presented improved accuracy in comparison to the CZM employing the bi-linear traction-separation law.

1 INTRODUCTION

Composite laminates offer noteworthy benefits over their metallic counterparts, especially for aerospace applications. High strength-to-weight ratio and easily configurable mechanical properties constitute some of the main reasons that have turn the researchers' attention towards them, in the past decades [1]. Extended efforts have been invested for the in-depth understanding of the mechanical and fracture behavior of the composite materials.

Fiber bridging is a commonly present phenomenon during the interlaminar fracture process or even debonding of composite joints. It can be defined as the residual connection between

failing adjacent plies though fibers or fiber bundles . The presence or absence of fiber bridging depends on various parameters such as the material and reinforcement orientation. Numerous works have been published focusing on the complex mechanism that leads to an unexpected failure behavior. Bridging can also result in a fracture toughness increment along the affected interfaces, which can be used in favor of the integrity of the structure [2].

Experimental studies include the investigation of the fiber orientation effect on the bridging behavior by Gong et. Al [3]. Hu et. Al. [4] worked on the effect of curing processes to the fiber bridging phenomenon. Furthermore, fatigue loading in combination with bridged fibers was studied by Jiang et al [5]. The integration into numerical simulations through the development of theoretical models accounting for fiber bridging has also been a research subject. Heidari-Rarani et al. [6] presented an approach based on the cohesive zone modeling (CZM) technique, where two simple bi-linear traction separation laws are superimposed to a tri-linear law, incorporating the effect of both the matrix and fibers. The latter model was further improved by Gong et al. [7] by altering the traction-separation responses to correspond to the fundamental failure behavior of the interface.

Although there is important number of studies available in the literature [8–12], numerical implementation for thermoplastic laminates considering fiber bridging is missing to the authors' knowledge. Thus, this paper focuses on the development of such a model in order to simulate the mixed mode fracture on co-consolidated thermoplastic laminates affected by bridging of carbon fibers. The numerical results were compared upon both experimental findings and numerical estimations with the employment of the traditionally used bi-linear traction separation law. It was found that the developed model managed to approach the experimental results in a good degree, improving the joint's strength prediction compared to the bi-linear law.

2 THEORETICAL BACKGROUND

The incorporation of the fiber bridging phenomenon to the cohesive material model was achieved through the employment of a recently proposed tri-linear traction-separation law by Gong et. Al. [7]. This section briefly describes the principle and theory of this cohesive zone model.

The representation of the mechanical behavior of the interface is described by a tri-linear traction-separation law (OABC) which accrues from the superposition of two simple bi-linear CZMs (fig. 1). For the representation of the matrix interface separation the bi-linear part (ODE) is employed. For $0\text{-}\delta_0$ displacement jump of the cohesive, linear elastic behavior is prescribed with K_1 stiffness, followed by the degradation part (DE) of the law. In the same principle, the effect of fiber bridging is modeled with another bi-linear law (OBC), where the onset of its degradation coincides with the total failure of the matrix interface. Finally, by superimposing the described components, a tri-linear traction separation law is obtained.

The global damage variable of the tri-linear CZM is divided as follows:

$$d = \begin{cases} 0, \delta \le 0 \\ \left(1 - \dfrac{K_{AB}}{K_0}\right)\left(1 - \dfrac{\delta_0}{\delta}\right), \delta_0 < \delta \le \delta_b \\ 1 - \dfrac{K_{BC}}{K_0}\left(1 - \dfrac{\delta_f}{\delta}\right), \delta_b < \delta \le \delta_f \\ 1, \delta \ge \delta_f \end{cases} \quad (1)$$

where K_0, K_{AB} and K_{BC} stand for the (OA), (AB) and (BC) lines' tangents respectively.

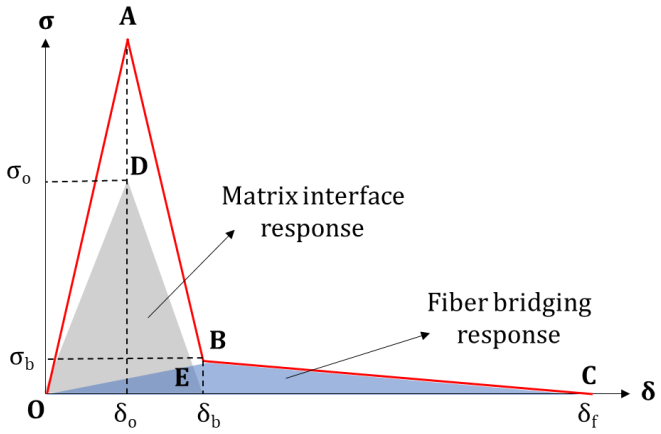

Figure 1. The modified Traction-Separation law.

3 APPROACH

The development of the final modified cohesive zone model for the co-consolidated laminates was consisted by experimental, analytical, and numerical parts. Initially, double cantilever beam coupons' tests, for mode I and edge notched flexure coupons' tests, for mode II were conducted. The data acquired from this first step were the fracture toughness values, as well as the resistance curves which are indicative of the bridging behavior of the specimens. However, the latter could not be generalized in any coupon for modeling of fiber bridging as these data are geometry dependent. To overcome this issue, a bridging law in each mode needed to be defined.

The technique followed to extract the bridging law and subsequently the bridging stress σ_b is described in the literature [13] and is comprised by a simplified procedure for measuring the crack opening displacement (COD) in DCB and the crack sliding displacement (CSD) in ENF coupons, eliminating the need for complex digital image correlation monitoring techniques during testing. The R-curves extracted from the two mechanical tests were introduced in two finite element models simulating the tests respectively. The fracture toughness values were obeying the R-curve behavior and the crack opening displacement could be measured numerically.

Finally, the numerical implementation of the modified mixed-mode CZM was followed through an already available LS Dyna's material and the results were validated upon available

test data. Furthermore, the numerical results that accrued from the modified model were compared to the output of a simple bilinear traction-separation law model.

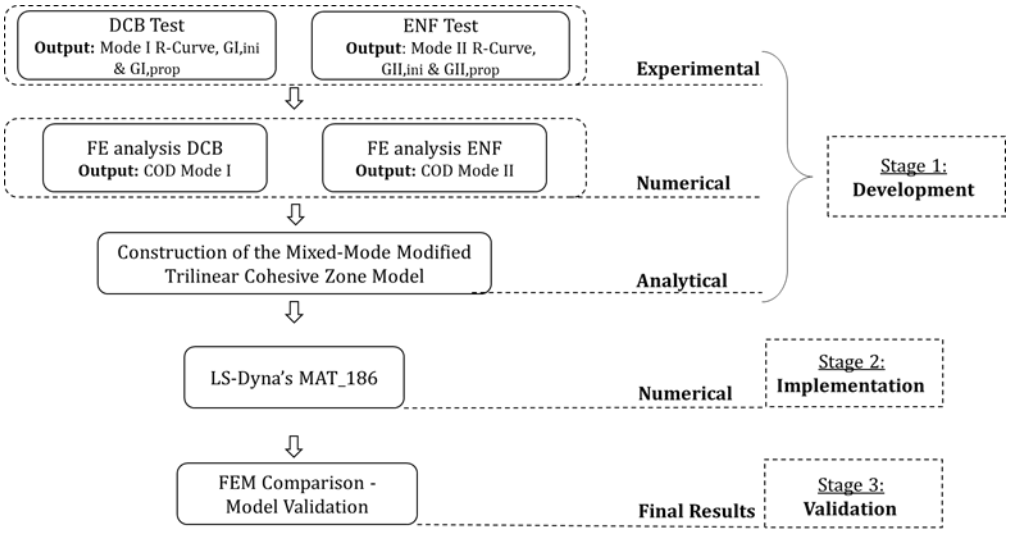

Figure 2. Model development flowchart.

The procedure described above was divided in three stages: development, implementation, and validation, for easier comprehension (Fig. 2). In the first step, the mandatory experimental, numerical, and analytical data are acquired. Subsequently these are used as input in the numerical models of the implementation stage and finally the results are compared and validated throughout the third stage.

4 DEVELOPMENT

4.1 Experimental

The mechanical testing of laminates in mode I loading conditions was performed according to the ASTM D5528-01 standard [14–16]. A total number of eight co-consolidated specimens were cut in 150 mm length, 25 mm width and 1.8 mm thickness for each substrate. The plies followed quasi-isotropic stacking $[0^0/45^0/90^0/45^0/\text{-}45^0]$s and the predefined crack was applied with a 63 mm Kapton film insert between the laminates. The prepreg material of the laminates was LM-PAEK based matrix, reinforced with TC1225 carbon fibers provided by Toray.

Piano hinge tabs were bonded at the edges of the cantilever beam in order to apply the opening load, according to the standard. The tests were held in room temperature conditions prescribing a constant crosshead displacement rate of 1 mm/min. During the loading of the coupons the crack propagation was optically monitored through a digital microscope. The fracture toughness values for each state of the propagation were obtained through the modified beam theory method.

The mechanical testing conducted on DCB showed similar results for all the coupons, Indicatively, in Fig. 3, a characteristic load-displacement curve is presented, while Fig. 4 depicts a characteristic R-curve for the co-consolidated laminates. The initial and propagation fracture toughness values in this case are roughly 1.1 N/mm and 2.1 N/mm respectively, while the length

of the crack propagation for the stabilization of the fracture toughness to a steady value, also defined as the bridging length, is about 40 mm.

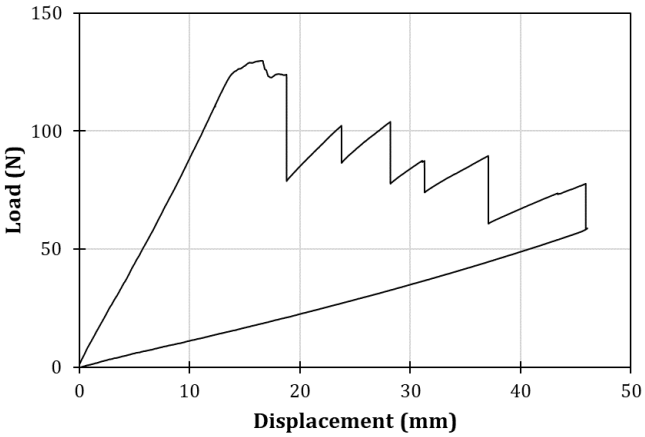

Figure 3. Characteristic Mode I Load-Displacement curve.

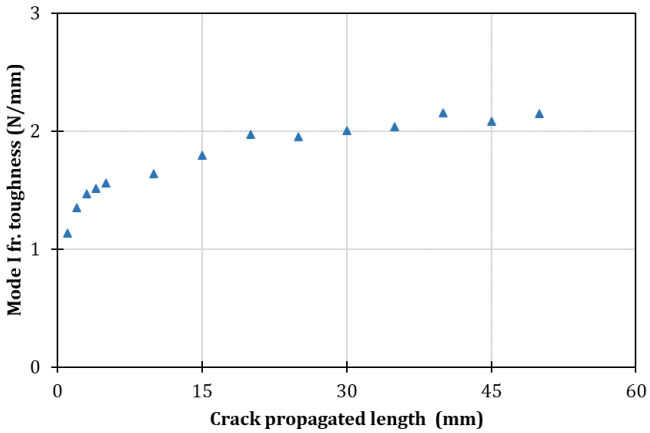

Figure 4. Characteristic Mode I R-Curve.

The mode II tests performed, complied to the AITM 1.0006 standard [17]. Six coupons of 115 mm by 25 mm dimensions and 45 mm predefined cracking were studied. In the same principle as mode I, the crack propagation under the constantly increasing load was monitored through a digital microscope [18]. The testing machine used was an MTS universal with 100 kN of load cell capacity. Fig. 5 depicts a characteristic load-displacement response of the ENF coupons as obtained from mode II testing.

Fig. 6 shows the characteristic fracture toughness – crack propagation curve, where the initiation G_{II} value was measured quite low at about 0.5 N/mm and the steady state G_{II} value at 2.6 N/mm. For this test, the bridging length was considerably lower from the mode I test, lying at 5 mm. It is noteworthy that due to the nature of the three-point bending test, the load – crack propagated length data recording proved to be quite difficult, rendering the acquisition of more data points on the R-curve impossible.

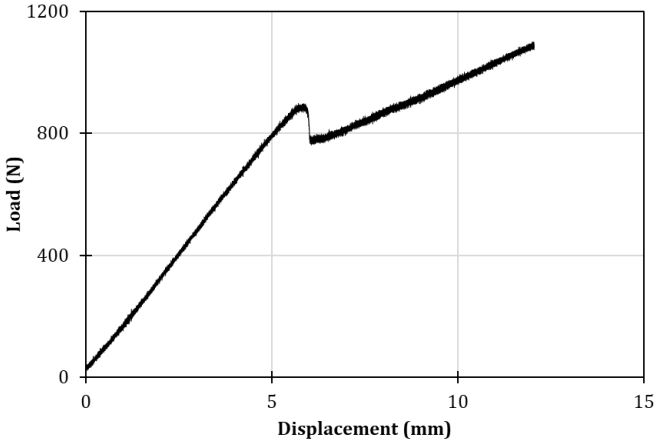

Figure 5. Characteristic Mode II Load-Displacement curve.

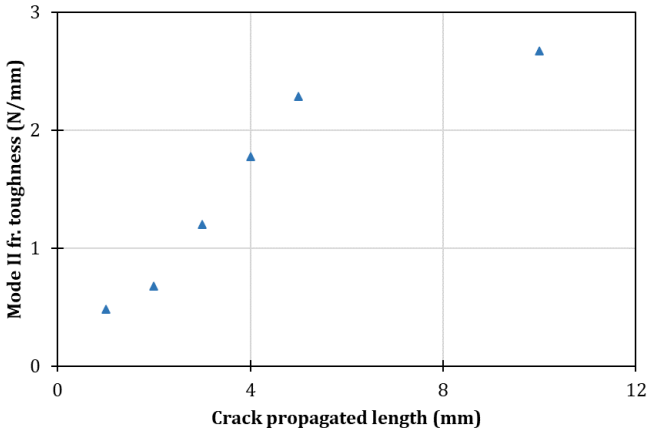

Figure 6. Characteristic Mode II R-Curve.

4.2 Numerical analysis

The numerical aspect of the present stage incorporates finite element simulations for the numerical estimation of the bridging law in DCB and ENF coupons. The numerical analyses were held in the commercial finite element suite, LS Dyna, using 8-noded reduced integrated solid elements for the composite laminates [19]. The numerical part also includes the development of the user defined routines in order to introduce the experimental R-curves in the DCB and ENF models (UMAT_RCurve). Simulations were performed in LS Dyna, while the proprietary scripting was written in FORTRAN 77 programming language and compiled through Intel Visual Fortran Compiler 2010. The developed subroutine was implemented through the LS Dyna's available material model UMAT43c, suitable for modelling three dimensional cohesive elements [19–21].

The mechanical response of this user defined model was exactly the same a simple bi-linear CZM, with the exception that the fracture toughness in each loading mode was not a constant value but was position dependent based on the experimental R-curves. In order to implement this, a cohesive element position reading algorithm had to be written.

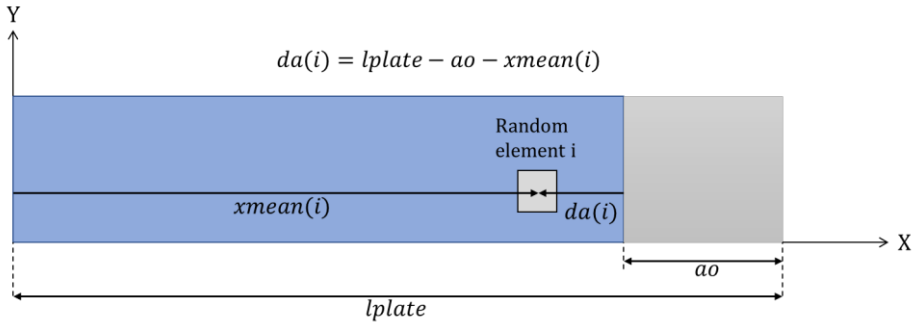

Figure 7. UMAT_RCurve routine element location algorithm schematic.

As an input the total coupon length ($lplate$) and the pre-cracked length (a_0) were required. Through an iterative procedure the nodal coordinates of the cohesive elements were obtained and subsequently the distance from the element's center to the crack tip ($da(i)$) was calculated (Fig. 7). By this means, the fracture toughness for each cohesive element is prescribed from the R-curve which also constitutes a subroutine's input.

The objective of this numerical step was to bypass the need for complex experimental monitoring techniques for the crack opening/sliding displacement by directly extracting the desired curve through finite element models of DCB and ENF. This procedure has been proposed in [13], however it has only been applied for mode I loading.

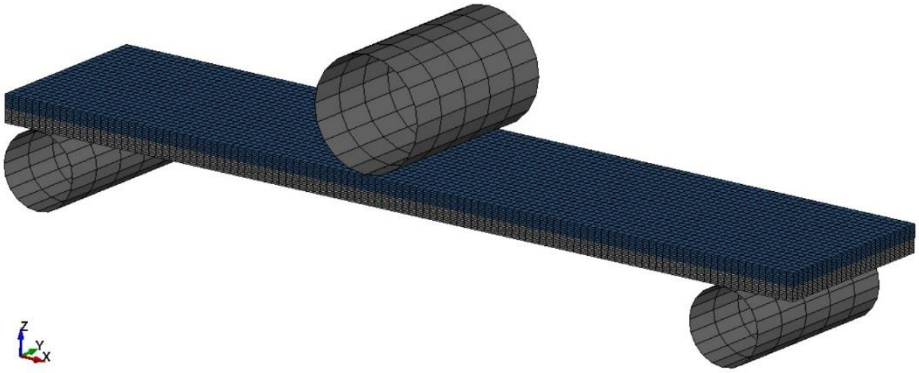

Figure 8. ENF specimen FE meshing.

Based on the procedure described the fracture toughness distribution along the cohesive elements on the interface of DCB specimen was prescribed. The lowest G value was applied at the crack-front elements, increasing according to the experimentally defined R-curve. Similarly, the same principle was applied to the ENF cohesive interface. By performing the numerical analyses for the two loading mode cases, the relative node displacements on the desired location were measured and the crack opening and sliding displacements were numerically obtained.

4.3 Analytical

In this part of the model development, the calculations for the mixed-mode tri-linear traction-separation law are included. As the first requirement, the bridging stress could be calculated from the differentiation of the fracture toughness by the crack opening displacement or crack sliding displacement, depending on the loading mode. The bridging stress – crack propagation curve could be plotted using the following equation:

$$\sigma_b = \frac{\partial G}{\partial \delta^*} \tag{2}$$

where δ^* stands for the crack opening or sliding displacement. K_1 and K_2 describe the stiffnesses for the two superimposed traction-separation laws to the corresponding loading mode. The K_1 value can be calculated by the following equation:

$$K_1 = \frac{2E_Z}{h} \tag{3}$$

where E_Z was the through the thickness laminates' stiffness, and h half of the DCB or ENF specimen thickness.

Ultimately, in this way the bridging stress – opening/sliding displacement curves could be drawn as shown in Fig. 9 and 10. The first points in these two diagrams corresponded to the mode I & II bridging strength, specifically $\sigma_{I,b} = 4.96\,MPa$ and $\sigma_{II,b} = \tau_b = 22.4\,MPa$. Consequently, after performing all the required calculations both for mode I and mode II loading conditions, the final traction-separation graph could be drawn as shown in Fig. 11.

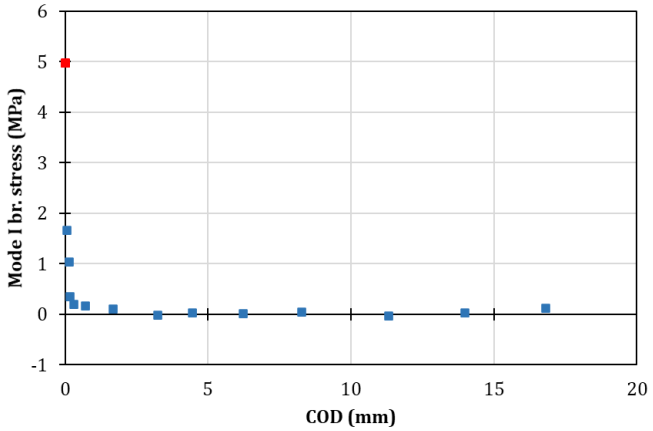

Figure 9. Mode I bridging stress – COD curve.

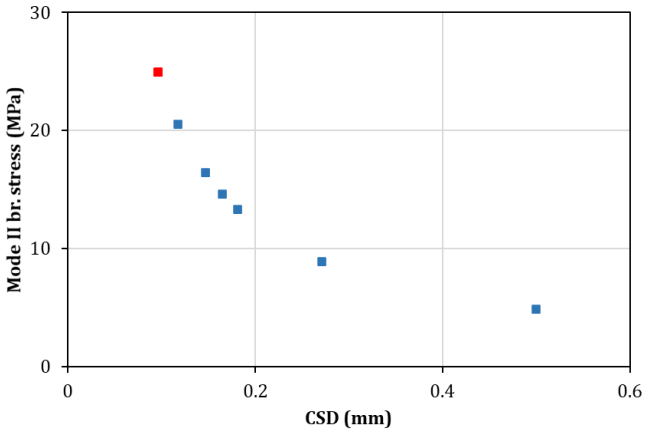

Figure 10. Mode II bridging stress – CSD curve.

5 IMPLEMENTATION

Numerical analyses were held in this stage to determine the behavior for the co-consolidated laminates under mixed mode loading. The simple bilinear CZM was simulated through LS Dyna's MAT_138 material model. The implementation of the tri-linear CZM was held through the employment of LS Dyna's MAT_186 (MAT_COHESIVE_GENERAL) material model, which allowed the definition of user-defined traction-separation laws by prescribing a normalized curve. Different cohesive responses can be prescribed for the two loading modes making the mixed-mode simulation possible.

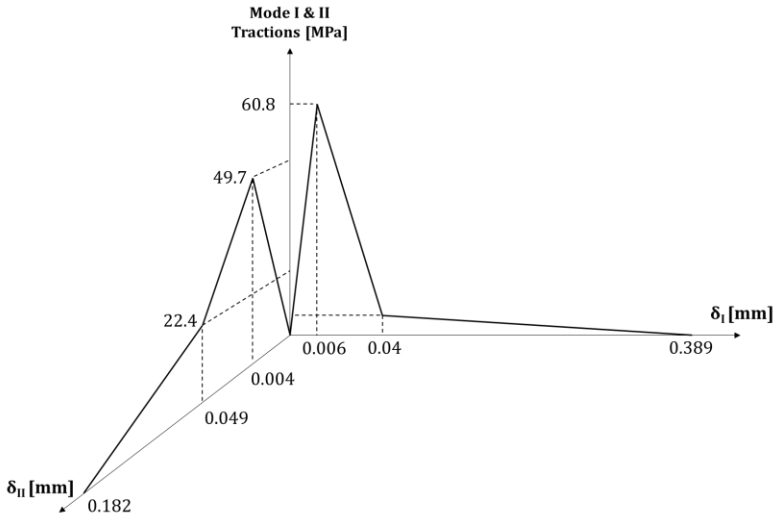

Figure 11. The final mixed-mode trilinear Traction-Separation law.

6 FINAL RESULTS & VALIDATION

In this section, the final mechanical responses of the mixed-mode SLS coupons from the numerical simulations are presented. The numerical results include the output data for the

trilinear CZM modeled interfaces and then compared to the bilinear modeled interface response and experimentally acquired data.

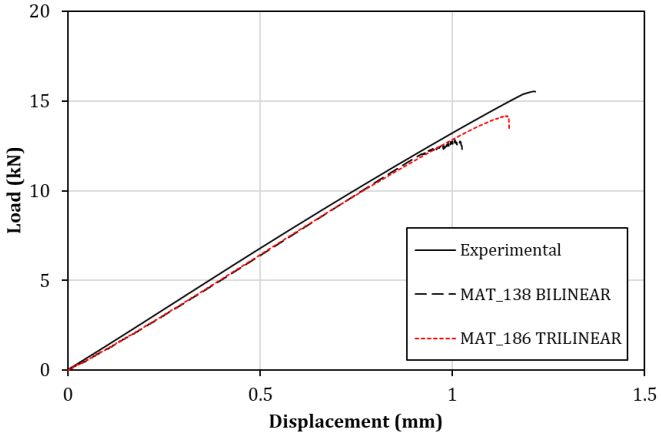

Figure 12. Experimental and numerical Load-Displacement curves' comparison.

Fig. 12 depicts the load displacement curves accrued from the numerical analyses. The experimentally obtained curve peaked at 16 MPa prior to failure. Significantly lower was the maximum load for the bilinearly modeled coupon. Such a difference was expected as MAT_138 didn't reckon in the fiber bridging effect, extensively present on the failed areas of the tested SLS specimens. The model based on the modified traction – separation law managed to approach the experimental behavior more accurately than the simple bilinear model. Although the load-displacement curve didn't fully capture the real-world mechanical behavior, considerable improvement was occurred.

7 CONCLUSIONS

Overall, the developed model was proved to be accurate for simulating the fiber bridging behavior of mixed-mode loaded co-consolidated thermoplastic laminates. Although the numerical results were not identical with the mechanical tests' data, the improvement over the traditional bilinear cohesive zone modeling was considerable. The trilinear traction-separation law managed to simulate the increased fracture properties due to the bridging of fibers. Furthermore, this procedure could potentially be applied apart from co-consolidated thermoplastic joints and interlaminar fracture, on thermoplastic welded joints.

The UMAT_RCurve subroutine was proved an efficient way to measure the crack opening/sliding displacements in both loading modes, as complex experimental monitoring techniques can be replaced while maintaining adequate accuracy.

Concluding, such a procedure was quite more complex in the development and implementation than the traditionally used traction-separation law. Additional steps, both numerical and analytical were required for the acquisition of the modified trilinear traction-separation law. Considering that, this technique should be used in cases that the fiber bridging phenomenon is quite extensive and affects the mechanical response of the joint noticeably.

Acknowledgment

The present study was conducted in the frame of the European research project TORNADO Clean Sky 2: "Innovative Disbond Arrest Features for Long Thermoplastic Welded Joints" (Grant Agreement No.: 101007494). Partners: RESCOLL, KVE Composites Group and University of Patras. Topic Manager: GKN Fokker

References

[1] Pantelakis S, Tserpes K, editors. Revolutionizing Aircraft Materials and Processes. Cham: Springer International Publishing; 2020. https://doi.org/10.1007/978-3-030-35346-9.

[2] Khan R. Fiber bridging in composite laminates: A literature review. Composite Structures 2019;229:111418. https://doi.org/10.1016/j.compstruct.2019.111418.

[3] Gong Y, Chen X, Li W, Zhao L, Tao J, Zhang J, et al. Delamination in carbon fiber epoxy DCB laminates with different stacking sequences: R-curve behavior and bridging traction-separation relation. Composite Structures 2021;262:113605. https://doi.org/10.1016/j.compstruct.2021.113605.

[4] Hu P, Pulungan D, Tao R, Lubineau G. Influence of curing processes on the development of fiber bridging during delamination in composite laminates. Composites Part A: Applied Science and Manufacturing 2021;149:106564. https://doi.org/10.1016/j.compositesa.2021.106564.

[5] Jiang L, Zhang Y, Gong Y, Li W, Ren S, Liu H. A new model characterizing the fatigue delamination growth in DCB laminates with combined effects of fiber bridging and stress ratio. Composite Structures 2021;268:113943. https://doi.org/10.1016/j.compstruct.2021.113943.

[6] Heidari-Rarani M, Shokrieh MM, Camanho PP. Finite element modeling of mode I delamination growth in laminated DCB specimens with R-curve effects. Composites Part B: Engineering 2013;45:897–903. https://doi.org/10.1016/j.compositesb.2012.09.051.

[7] Gong Y, Hou Y, Zhao L, Li W, Zhang J, Hu N. A modified mode I cohesive zone model for the delamination growth in DCB laminates with the effect of fiber bridging. International Journal of Mechanical Sciences 2020;176:105514. https://doi.org/10.1016/j.ijmecsci.2020.105514.

[8] Fu C, Wang X. Simulating delamination in composite laminates involving large scale fiber bridging based on the mixed-mode three-linear cohesive zone model. Theoretical and Applied Fracture Mechanics 2022;117:103164. https://doi.org/10.1016/j.tafmec.2021.103164.

[9] Canal LP, Alfano M, Botsis J. A multi-scale based cohesive zone model for the analysis of thickness scaling effect in fiber bridging. Composites Science and Technology 2017;139:90–8. https://doi.org/10.1016/j.compscitech.2016.11.027.

[10] Riccio A, Russo A, Raimondo A, Sellitto A. A Numerical Assessment of Fibre Bridging Influence on Composite Panels Skin-stringer Debonding. Procedia Engineering 2016;167:56–63. https://doi.org/10.1016/j.proeng.2016.11.669.

[11] Lindhagen JE, Gamstedt EK, Berglund LA. Application of bridging-law concepts to short-®bre composites Part 3: Bridging law derivation from experimental crack pro®les. Composites Science and Technology 2000:12.
[12] Riccio A, Russo A, Sellitto A, Raimondo A. Development and application of a numerical procedure for the simulation of the “Fibre Bridging” phenomenon in composite structures. Composite Structures 2017;168:104–19. https://doi.org/10.1016/j.compstruct.2017.02.037.
[13] Gong Y, Chen X, Tao J, Zhao L, Zhang J, Hu N. A simple procedure for determining the mode I bridging stress of composite DCB laminates without measuring the crack opening displacement. Composite Structures 2020;243:112147. https://doi.org/10.1016/j.compstruct.2020.112147.
[14] ASTM International. D 5528 – 01 Standard Test Method for Mode I Interlaminar Fracture Toughness of Unidirectional Fiber-Reinforced Polymer Matrix Composites n.d.
[15] Moutsompegka E, Tserpes K, Noeske M, Schlag M, Brune K. Experimental Investigation of the Effect of Pre-Bond Contamination with Fingerprints and Ageing on the Fracture Toughness of Composite Bonded Joints. Appl Compos Mater 2019;26:1001–19. https://doi.org/10.1007/s10443-019-09763-9.
[16] Moutsompegka E, Polydoropoulou P, Tserpes KI, Tornow C, Schlag M, Brune K, et al. THE EFFECTS OF PRE-BOND CONTAMINATION WITH DE-ICING FLUID ON THE MODE-I AND MODE-II FRACTURE TOUGHNESS OF COMPOSITE BONDED JOINTS n.d.:12.
[17] Airbus Industrie Test Method. AITM 1.0006 Determination of interlaminar fracture toughness energy Mode II n.d.
[18] Anyfantis KN, Tsouvalis NG. Characterization of Fiber Bridging in Mode II Fracture Growth of Laminated Composite Materials. AMM 2010;24–25:245–50. https://doi.org/10.4028/www.scientific.net/AMM.24-25.245.
[19] Hallquist JO, editor. LS-DYNA: theory manual. Livermore, Calif: Livermore Software Technology Corp; 2006.
[20] Floros I, Tserpes K. Numerical simulation of quasi-static and fatigue debonding growth in adhesively bonded composite joints containing bolts as crack stoppers. The Journal of Adhesion 2021;97:611–33. https://doi.org/10.1080/00218464.2019.1690473.
[21] Tserpes K, Floros I. Fatigue crack growth simulation in adhesively bonded composite joints. Fatigue Fract Eng Mater Struct 2019;42:1430–40. https://doi.org/10.1111/ffe.12969.